NANO LETTERS

Letter

pubs.acs.org/NanoLett

Large Area Directed Self-Assembly of Sub-10 nm Particles with Single Particle Positioning Resolution

Mohamed Asbahi,[†] Shafigh Mehraeen,[‡] Fuke Wang,[†] Nikolai Yakovlev,[†] Karen S. L. Chong,[†] Jianshu Cao,[‡] Mei Chee Tan,[*,§] and Joel K. W. Yang[*,†,§]

[†]Institute of Materials Research and Engineering, A*STAR, 3 Research Link, Singapore 117602

[‡]Department of Chemistry, Massachusetts Institute of Technology, Cambridge, Massachusetts 02139, United States

[§]Pillar of Engineering Product Development, Singapore University of Technology and Design, 8 Somapah Road, Singapore 487372

Supporting Information

ABSTRACT: Directed self-assembly of nanoparticles (DSA-n) holds great potential for device miniaturization in providing patterning resolution and throughput that exceed existing lithographic capabilities. Although nanoparticles excel at assembling into regular close-packed arrays, actual devices on the other hand are often laid out in sparse and complex configurations. Hence, the deterministic positioning of single or few particles at specific positions with low defect density is imperative. Here, we report an approach of DSA-n that satisfies these requirements with less than 1% defect density over micrometer-scale areas and at technologically relevant sub-10 nm dimensions. This technique involves a simple and robust process where a solvent film containing sub-10 nm gold nanoparticles climbs against gravity to coat a prepatterned template. Particles are placed individually into nanoscale cavities, or between nanoposts arranged in varying degrees of geometric complexity. Brownian dynamics simulations suggest a mechanism in which the particles are pushed into the template by a nanomeniscus at the drying front. This process enables particle-based self-assembly to access the sub-10 nm dimension, and for device fabrication to benefit from the wealth of chemically synthesized nanoparticles with unique material properties.

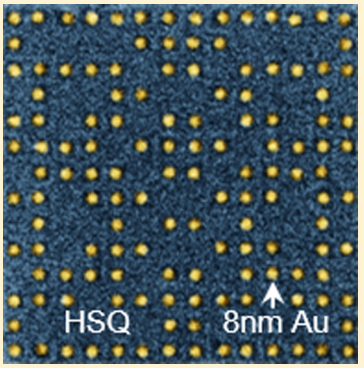

KEYWORDS: *directed self-assembly, template assisted self-assembly, single particle positioning, single particle resolution, gold nanoparticles, close packing*

The achievements in semiconductor manufacturing and device fabrication have relied solely on top-down lithographic techniques. As extreme device miniaturization continues, the tools and processes required could incur unsustainably high capital costs. Continued miniaturization beyond 10 nm dimensions could exploit quantum effects with materials that exhibit extraordinary properties, leading to more sophisticated, and power efficient devices.[1,2] At these length scales, conventional patterning techniques are faced with physical limitations in resolution that are challenging to overcome. On the other hand, colloidal synthesis has reached a mature level capable of producing sub-10 nm particles in a variety of materials and geometries.[3] Introducing these particles as active elements at strategic positions on a lithographically defined substrate could potentially create devices that have enhanced functionalities, and reduced production costs.[4−6] A technological barrier though is in the reliable positioning of single sub-10 nm particles with high yield over large areas.

Positioning of single particles into predefined surface topography requires the guidance of capillary forces at the receding meniscus of a host liquid. Distinct from the formation of close-packed super lattices of nanoparticles, single-particle resolution positioning finds potential applications in complex structure fabrication that requires some form of top-down patterning, and assemblies with locally varying densities. Although single-particle positioning of large (>50 nm) particles from liquid suspensions has been demonstrated using a moving macroscopic meniscus over a prepatterned template,[7,8] this approach causes particles at sub-10 nm dimensions to pack randomly or agglomerate.[9,10] At these length scales, particle dynamics is less influenced by the capillary force of the macromeniscus, as the latter exhibits a large capillary length compared to the particle size. Instead, at such small length scales, Brownian and pair potential forces strongly dominate thus creating the undesirable random assembly of particles.

In the present work, we introduce a novel method and propose a mechanism that enables sub-10 nm particles to be controllably positioned into lithographically defined templates. On the basis of the spreading laws of liquids on solid surfaces,[11−13] we create conditions suitable for a thin film of hexane to form and confine a single layer of ∼8 nm diameter Au nanoparticles (AuNPs) on the substrate surface. In contrast to the approach of chemical functionalization and covalent binding to capture particles,[14] our approach relies purely on

Received: June 9, 2015
Revised: August 14, 2015

DOI: 10.1021/acs.nanolett.5b02291
Nano Lett. XXXX, XXX, XXX−XXX

topographical features of the template, thus avoiding surface functionalization processes that could be sensitive to contamination. It overcomes the outstanding resolution limitation of capillary-driven approaches, thus bringing DSA-n into the sub-10 nm regime.

The key concept of the spreading mediated directed self-assembly of nanoparticles (SMDSA-n) is illustrated in Figure 1a with the corresponding scanning-electron micrograph (SEM) image in Figure 1b. AuNPs were synthesized by solution chemistry with an average core diameter of ∼8 nm.[15] They were suspended in hexane after being sterically stabilized with a shell of oleylamine ligands which leads to a total particle diameter of ∼12 nm. The template was fabricated by patterning a 20 nm thick film of hydrogen silsesquioxane (HSQ) negative tone resist on a Si substrate, using a 100 keV electron beam lithography system (EBL).[16,17] The sample was developed for 1 min in an aqueous solution of 1% NaOH and 4% NaCl, followed by rinsing in deionized water for 1 min and blow-drying with a nitrogen gun.[18] Samples were treated for 5 min in a UV ozone cleaner before use in the SMDSA-n process. To initiate the SMDSA-n process, that is, the spreading stage, one

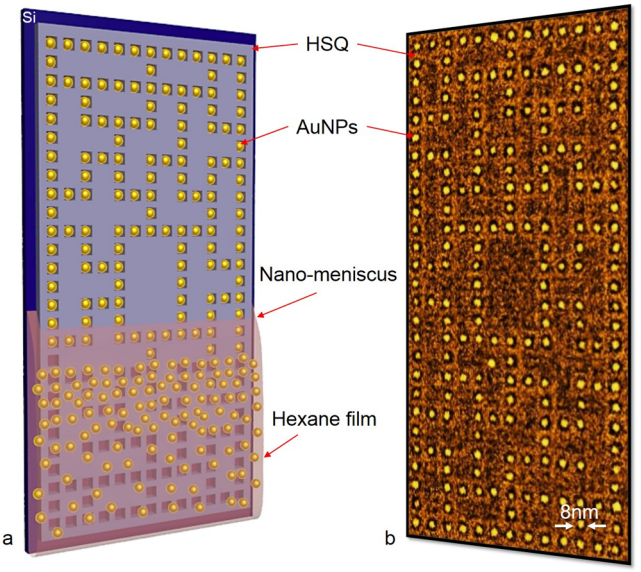

Figure 1. (a) Schematic illustration of a spreading-mediated directed self-assembly of nanoparticles (SMDSA-n) process. SMDSA-n achieves the positioning of single sub-10 nm particles from a solvent solution into an arbitrary topographical template consisting of nanoscale cavities fabricated in hydrogen silsesquioxane (HSQ) resist. Gold nanoparticles (AuNPs) are confined above the template surface and pushed into the cavities by a nanomeniscus as it sweeps downward during the drying of hexane. (b) False-colorized scanning-electron micrograph shows a mirror image of the schematic based of 8 nm AuNPs trapped in an arbitrary and sparse arrangement of nanocavities in a HSQ template.

of the sample edges was brought in contact with the surface of the AuNP bath leading to the formation of a macromeniscus between the sample and the liquid interface (see Supporting Information for details). The concentration of AuNPs within the bath solution was measured using ultraviolet−visible Spectroscopy (UV−vis) and the concentration was 1.67 × 10^{13} cm^{-3}. The system, bath and sample, were kept in a partially covered chamber to maintain a hexane-rich environment. Hexane was allowed to escape the chamber through a ∼2 mm

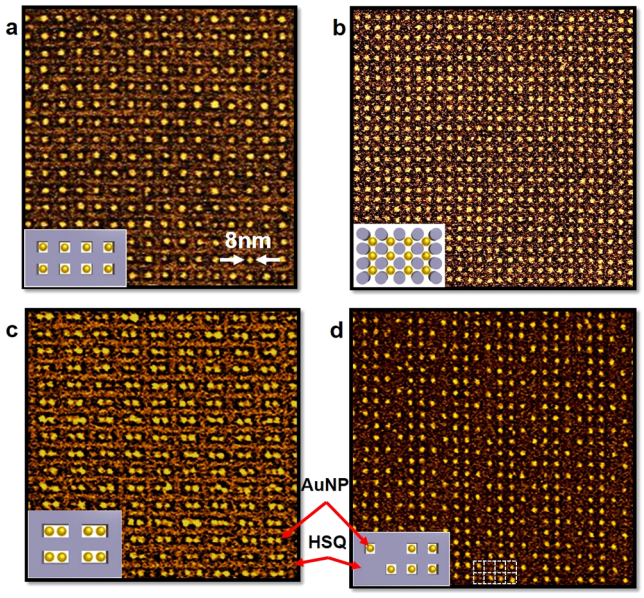

Figure 2. Scanning electron micrographs showing 8 nm AuNPs directed to assemble onto HSQ templates of varying configurations. The insets show schematics of the samples design. Single particles occupying a grid of 17 × 17 nm^2 square cavities are shown for two different pattern densities (a and d). (b) Single particles trapped between 10 nm diameter posts arranged in a square array. (c) Two particles per rectangular cavity of 17 × 34 nm^2.

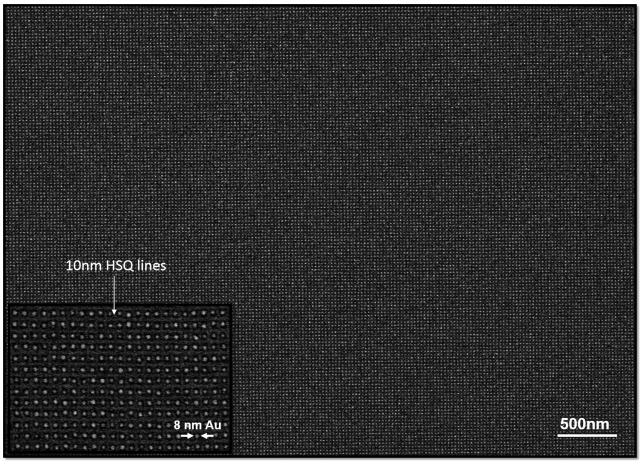

Figure 3. SEM image of a defect free assembly of AuNPs with single particle resolution on a HSQ template in a square array of 200 × 150 cavities with 27 nm center-to-center distance. Higher magnification of sample is shown in the inset.

diameter opening in the top lid. The setup created suitable conditions for a thin film of AuNPs in hexane to spread and climb up the substrate surface (Supporting Information Figure S1b). Within the first ∼20 min of the film formation, that is, when the climbing front reaches the top edge of the sample, we observed that the concentration of AuNPs within the film was not sufficient to achieve full coverage of the template. Therefore, samples were kept in contact with the bath for 1 h to increase the concentration of AuNP in the film. While hexane continuously evaporates, AuNPs accumulate in the film to achieve a high concentration within the film that ensures full coverage of the patterned region of the substrate. The thickness of the climbing film was estimated by ellipsometry to be ∼100

DOI: 10.1021/acs.nanolett.5b02291
Nano Lett. XXXX, XXX, XXX−XXX

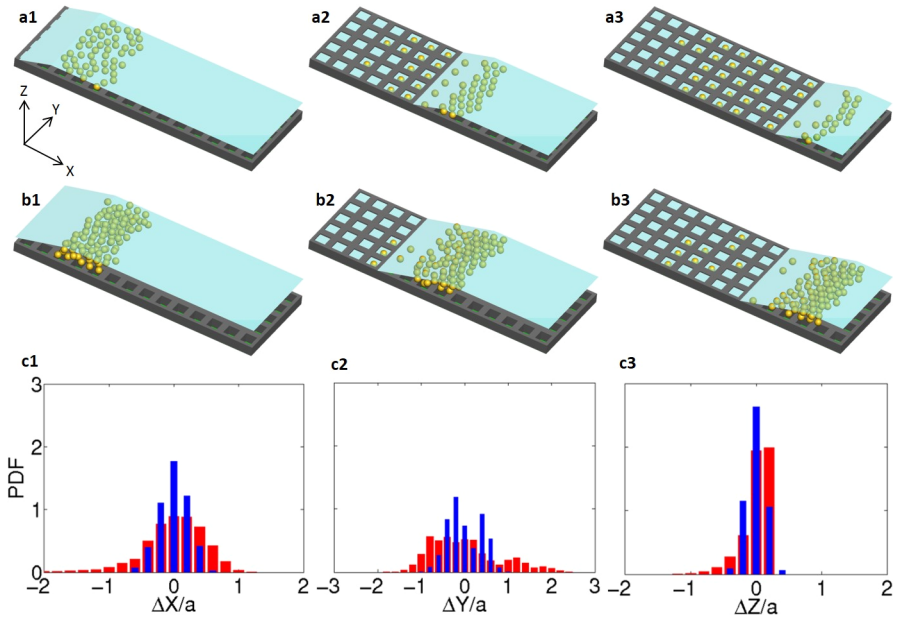

Figure 4. Progression of Brownian dynamics simulations of DSA-n of monolayer (a) and double-layer (b) sub-10 nm particles into a template, from left to right, suggesting that reducing the liquid thickness enhances deposition coverage, that is, successful filling of the nanoscale cavities. We attribute this coverage enhancement to the PDFs of *x*, *y*, and *z* positional variation (from left to right) averaged over 10 particles, which are wider in monolayer (red) than that in double layer (blue) shown in panel (c), (a = 5 nm is the particle radius used in the simulation).

nm. It is important to note that the volume of hexane escaping out of the experimental system during the self-assembly process is very small compared to the bulk volume of the bath, that is, the change of the concentration of AuNPs within the bath is negligible and does not influence the concentration within the climbing film.

The sample was then raised above the suspension bath and left to dry for 30 min in the hexane rich environment. During this process, the evaporation of hexane results in a thin but uniform film. Eventually nanomenisci, that is, receding drying fronts of this thin film, form at the top of the sample and spread throughout the sample to finally push the particles into the template cavities, as shown in Figure 1a. The SEM image in Figure 1b demonstrates the capability of SMDSA-n in positioning single AuNPs into a predetermined arrangement of nanocavities on a HSQ template.

As AuNPs naturally self-assemble into hexagonally close-packed arrays,[15,16,19] a first test of the effectiveness of templates was to *direct* particles to assemble in a square lattice instead. Figure 2 shows single as well as double AuNPs located in cavities or trapped between 4 HSQ posts. As illustrated by the inset schematics, single particles occupying a grid of 17 × 17 nm^2 square cavities are shown for two different occupation densities in Figure 2a and d. Single particles trapped between 10 nm diameter posts arranged in a square array are also shown in Figure 2b. By elongating the cavity of the template, two particles can be trapped in rectangular cavities of 17 × 34 nm as shown in Figure 2c. These results demonstrate the potential of SMDSA-n in positioning individual nanoparticles into predefined locations to form 2D lattices with negligible defects using templates of different geometric complexity. Figure 2d illustrates AuNPs assembled into a template consisting of repeating unit cells of 6 nanocavities in an asymmetric arrangement, as shown in the inset. Note that at the pattern resolutions shown here, SEM inspection becomes increasingly challenging. Nonetheless the high secondary electron yield from AuNPs compared to its surrounding provide sufficient signal-to-noise ratio to be identified in the SEM images.

Unlike previous work where defect-free regions in templates are limited to tens of repeat units,[20] the present process is remarkably capable of defect free assemblies over hundreds of repeat units. Figure 3 shows an example of single particles assembled within 17 × 17 nm^2 square HSQ arranged within an array of 200 × 150 cavities with negligible defects. This result is comparable to template-assisted self-assembly of large particles,[7,8] and is now made possible for sub-10 nm particles with this new process.

Because the particles are too small for optical microscopy tracking during the assembly process, we obtain insight on the mechanism that leads to successful assembly through Brownian dynamics (BD) simulations (see Supporting Information for details). The simulations included the main particle−particle interactions (Hamaker potential representing long-range attraction, and short-range repulsion), template−particle interactions (short-range repulsion), and fluid−particle interactions (capillary forces from surface tension applied to particles at the fluid free surface).[21] We compare BD simulation results of solvent thickness of 15 and 30 nm with a constant AuNP concentration and nanomeniscus contact angle of 12 deg[22] between hexane and the substrate. Snapshots of the simulations for two liquid thicknesses, 15 and 30 nm, as the nanomeniscus recedes across the template are shown in Figure 4a and b, respectively. The sequence in Figure 4a indicates that the nanoparticles confined in the 15 nm thin liquid film will transition from an initial random arrangement into a semi-ordered monolayer above the template as they are swept across by the nanomeniscus. The formation of this packed monolayer is necessary to initiate the defect-free filling of the nanocavities, evidenced by the initial vacancy defects in the first few rows. For clear visualization of the nanomeniscus, we intentionally left the first two rows of cavities vacant with an initially random distribution of particles starting from row 3 onward in *x*

DOI: 10.1021/acs.nanolett.5b02291
Nano Lett. XXXX, XXX, XXX−XXX

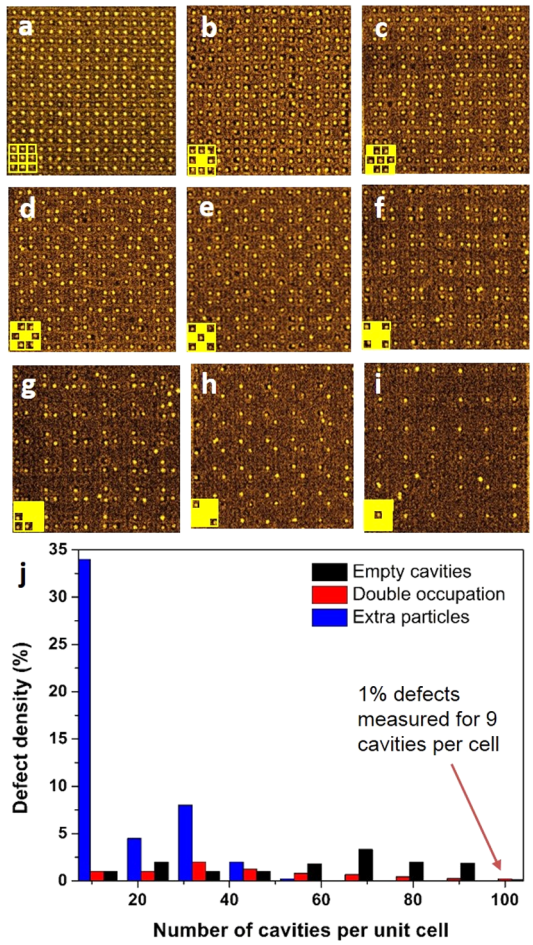

Figure 5. SEM images showing 8 nm diameter AuNPs assembled into HSQ templates consisting of cells with varying number of cavities from 9 to 1 as shown in the inset. From (a) to (i), the number of cavities for each unit cell was sequentially reduced by one. (j) Histogram of the different types of defects densities as a function of the number of cavities per unit cell measured on arrays of 10 × 10 cells.

direction. During the successful filling that follows, particles are first separated from the monolayer and prepositioned above the nanocavities before being slotted in by the downward force of the nanomeniscus (see movies in Supporting Information). As the film gets depleted of particles, vacancy defects begin to appear.

Although it is important to have a high concentration of particles at the receding nanomeniscus in order to minimize the defect density resulting from the solvent evaporation dynamics, defect-free filling also requires that the thin film confines only a single layer of particles. As seen in Figure 4b, a 30 nm thick film that supports two layers of particles hinders particles deposition; thus, it increases vacancy defects and lowers filling yield. This effect is attributed to the formation of a semicrystalline phase of particles with hexagonal ordering immediately in front of the moving nanomeniscus. In this phase, the energetic barrier to separate individual particles for prepositioning above the cavities is higher due to the larger number of nearest neighbors interactions at the front line (see Supporting Information for details).

To further investigate the role of liquid thickness and the degree of confinement on particles motion and DSA-n, we look at positional variation about the mean in x, y, and z directions for particles using BD simulations. Figure 4c illustrates the probability distribution function (PDF) of positional variation averaged over 10 randomly selected particles from BD simulations using thin (monolayer, red) and thick (double-layer, blue) arrangements. Results shown in Figure 4c imply that PDF of positional variations for particles in thin monolayer arrangement is generally wider than that for particles in the double-layer arrangement. We correlate this variation in PDF to higher energetic barriers associated with particle separation from a double-layer arrangement with crystalline phase morphology followed by the insertion into the cavities. Results shown in Figure 4c corroborates with experimental observation shown in Figure 3 indicating the importance of thin film and confinement in increasing the yield of DSA of sub-10 nm particles.

It is noteworthy that contact angle also plays a significant role in DSA-n performance. A series of systematic BD simulations for contact angles of 10, 30, and 50 degrees at different liquid thicknesses (15 and 30 nm) suggest that large liquid thickness and contact angles lead to large, hexagonally ordered clusters in front of nanomeniscus that hinders particle deposition; thus increasing vacancy defects. However, small fluid thickness and contact angle confine the particles to the least possible nearest neighbor interactions, facilitating deposition by the nanomeniscus, which further enhances DSA-n coverage.

Figure 5 presents SEM images and defect analysis in positioning AuNPs into templates of varying area densities of cavities. The templates are based on unit cells of different cavity arrangements (shown in the inset) that was repeated to form an array of 10 × 10 cells. From Figure 5a to i, we varied the cavity density by sequentially removing one cavity from each unit. Cavity size was kept nominally constant at ~17 × 17 nm^2. This figure illustrates the potential of SMDSA-n in positioning single sub-10 nm particles in more complex template geometries. Three different classifications of defects were observed, that is, (1) empty cavities, (2) double occupancy (2 particles per cavity), and (3) extra particles (particles attached on top of HSQ between the cavities). The array with the maximum particle density (Figure 5a) showed the lowest defect levels of less than 1% as also observed in Figure 3. As we can see in the histogram (Figure 5j), the empty cavities and double occupancy defects were present for all cavity densities but at low levels (less than 3%). The extra particle defects start appearing only when the number of cavities was reduced to less than 4 per unit cell. This last type of defects is mainly due to the surface corrugations in the HSQ arising from the raster scanning of the electron beam during exposure, noticeable in Figure 5g–i. The attachment of particles due to these corrugations illustrates the sensitivity of the assembly process to surface topography, which can be improved by careful patterning strategies. Moreover, particles size variations is at the origin of the double occupation defects as most of the observed defects of this kind were obtained with two nanoparticles with different sizes or with two similar-size particles but smaller than the mean particle diameter. Hence, we expect defect levels to be further reduced with more uniform particle sizes and optimized template topography. Moreover, the size distribution of particles responsible for double occupation defects is a clear indicator that SMDSA-n process is suitable for a wide range of particle size as long as gravitational force is small enough to act against the film climbing. Other particle shapes such as nanorods may also give good results while the above condition is met; however, due to different geometrical symmetry, more complex

DOI: 10.1021/acs.nanolett.5b02291
Nano Lett. XXXX, XXX, XXX−XXX

templates will be needed to achieve similar results as with spherical nanoparticles.

The self-assembly of sub-10 nm particles in the presence of surface topography is typically dominated by high defect densities and random particle arrangements. The results reported here outline the important factors to achieve successful positioning of single sub-10 nm particles guided by surface topography. The process enables the formation of a thin liquid that confines a monolayer of particles and a moving nanomeniscus that slots particles into the template. Although experiments were based on spherical Au nanoparticles, we expect this process to be applicable to other types and shapes of nanoparticles, for example, quantum dots. This technique of spreading-mediated directed self-assembly of nanoparticles SMDSA-n can be further scaled up to macroscopic areas through optimized coating processes and precise control of chamber conditions. In addition to enabling precise positioning of particles for device fabrication with advanced functionalities, our results provide inroads to the experiment and modeling of particle-template interactions at ultrasmall dimensions.

■ ASSOCIATED CONTENT

Supporting Information

The Supporting Information is available free of charge on the ACS Publications website at DOI: 10.1021/acs.nanolett.5b02291.

Experimental methods (template fabrication and process flow of SMDS-A-n), Brownian dynamics simulations, comparison of energy barrier in particle removal between monolayer and double-layer arrangement using a lattice model, Figures S1−S3. (PDF)

Movie showing single-layer nanoparticle filling of the nanocavities. (AVI)

Movie showing double-layer nanoparticle filling of the nanocavities. (AVI)

■ AUTHOR INFORMATION

Corresponding Authors

*E-mail: joel_yang@sutd.edu.sg.

*E-mail: meichee.tan@sutd.edu.sg.

Notes

The authors declare no competing financial interest.

■ ACKNOWLEDGMENTS

This work was supported by the Agency for Science, Technology and Research (A*STAR) in Singapore. The work made use of the SERC nano Fabrication, Processing and Characterization (SnFPC) facilities in the Institute of Materials Research and Engineering (IMRE). S.M., J.C., and M.C.T. also gratefully acknowledge the support from the MIT-SUTD Postdoctoral Fellows Program. M.A. acknowledges funding through project code IMRE/13-2B0278 (A*STAR Nanoimprint Foundry).

■ REFERENCES

(1) Talapin, D. V.; Lee, J. S.; Kovalenko, M. V.; Shevchenko, E. V. *Chem. Rev.* **2010**, *110*, 389−458.

(2) Fan, J. A.; Bao, K.; Sun, L.; Bao, J. M.; Manoharan, V. N.; Nordlander, P.; Capasso, F. *Nano Lett.* **2012**, *12*, 5318−5324.

(3) Glotzer, S. C.; Solomon, M. J. *Nat. Mater.* **2007**, *6*, 557−562.

(4) Anikeeva, P. O.; Halpert, J. E.; Bawendi, M. G.; Bulovic, V. *Nano Lett.* **2009**, *9*, 2532−2536.

(5) Klein, D. L.; Roth, R.; Lim, A. K. L.; Alivisatos, A. P.; McEuen, P. L. *Nature* **1997**, *389*, 699−701.

(6) Sargent, E. H. *Adv. Mater.* **2008**, *20*, 3958−3964.

(7) Kraus, T.; Malaquin, L.; Schmid, H.; Riess, W.; Spencer, N. D.; Wolf, H. *Nat. Nanotechnol.* **2007**, *2*, 570−6.

(8) Xia, Y. N.; Yin, Y. D.; Lu, Y.; McLellan, J. *Adv. Funct. Mater.* **2003**, *13*, 907−918.

(9) Deegan, R. D.; Bakajin, O.; Dupont, T. F.; Huber, G.; Nagel, S. R.; Witten, T. A. *Nature* **1997**, *389*, 827−829.

(10) Yunker, P. J.; Still, T.; Lohr, M. A.; Yodh, A. G. *Nature* **2011**, *476*, 308−311.

(11) Degennes, P. G. *Rev. Mod. Phys.* **1985**, *57*, 827−863.

(12) Heslot, F.; Fraysse, N.; Cazabat, A. M. *Nature* **1989**, *338*, 640−642.

(13) Wasan, D. T.; Nikolov, A. D. *Nature* **2003**, *423*, 156−159.

(14) Abramson, J.; Palma, M.; Wind, S. J.; Hone, J. *Adv. Mater.* **2012**, *24*, 2207−2211.

(15) Lau, C. Y.; Duan, H.; Wang, F.; He, C. B.; Low, H. Y.; Yang, J. K. *Langmuir* **2011**, *27*, 3355−60.

(16) Asbahi, M.; Lim, K. T.; Wang, F.; Duan, H.; Thiyagarajah, N.; Ng, V.; Yang, J. K. *Langmuir* **2012**, *28*, 16782−7.

(17) Asbahi, M.; Mehraeen, S.; Lim, K. T.; Wang, F.; Cao, J.; Tan, M. C.; Yang, J. K. *Nano Lett.* **2014**, *14*, 2642−6.

(18) Yang, J. K. W.; Berggren, K. K. *J. Vac. Sci. Technol., B* **2007**, *25*, 2025−2029.

(19) Bigioni, T. P.; Lin, X. M.; Nguyen, T. T.; Corwin, E. I.; Witten, T. A.; Jaeger, H. M. *Nat. Mater.* **2006**, *5*, 265−70.

(20) Jiang, L.; Wang, W. C.; Fuchs, H.; Chi, L. F. *Small* **2009**, *5*, 2819−2822.

(21) Mehraeen, S.; Asbahi, M.; Fuke, W.; Yang, J. K.; Cao, J.; Tan, M. C. *Langmuir* **2015**, *31*, 8548−57.

(22) Drummond, C. J.; Chan, D. Y. C. *Langmuir* **1997**, *13*, 3890−3895.

DOI: 10.1021/acs.nanolett.5b02291
Nano Lett. XXXX, XXX, XXX−XXX